https://doi.org/10.32603/1993-8985-2019-22-3-74-87
УДК 621.396.96

Sergey R. Heister[1]✉, Thai T. Nguyen[2]

[1] Group of Manufacturing Technologies and Aeronautical Engineering AEROMASH
Minsk, Belarus

[2] Belarusian State University of Informatics and Radioelectronics
6, P. Brovki Str., 220013, Minsk, Belarus

MATHEMATICAL MODELS OF THE RADAR SIGNAL REFLECTED FROM A HELICOPTER MAIN ROTOR IN APPLICATION TO INVERSE SYNTHESIS OF ANTENNA APERTURE

Abstract

Introduction. *The problem of aircraft recognition can be solved on the basis of the formation of radar portraits that reflect the characteristic structural features of aerial vehicles. Radar portraits based on images of the propellers of aerial vehicles have high informativeness. On the basis of such images, the number and relative position of the propeller blades, as well as the direction of their rotation, can be determined. Such images may be obtained on the basis of mathematical models constructed from reflected signals.*

Objective. *The aim of the work is to develop mathematical models for the radar signal reflected from the main rotor of a helicopter applied to inverse synthetic aperture radar (ISAR).*

Methods and materials. *ISAR processing is used to produce a radar image of a rotor in a radar with a monochromatic probing signal. The rotor blades in the models are approximated by different geometric shapes. The models used to describe the reflection from the rotors of helicopters differ significantly from those used to describe fixed-wing aircraft propellers. In the process of moving through the air, each helicopter rotor blade performs characteristic movements (flapping, lead-lag motion, torsion), as well as flexing in a vertical plane. Such movements and flexings of the blades influence the phase of the radar signal deflected from the main rotor. When developing an ISAR algorithm for imaging the main rotor, the phase change must accurately account for the reflected signal.*

Results. *In the centimetre wavelength range, the mathematical model of the signal reflected from the main helicopter rotor as a system of blades is most accurately described if each blade is represented as a set of isotropic reflectors located on the leading and trailing edges of the main rotor blades. The distinct features of the actual signal are more closely approximated by a model that takes the flapping movements and curved shapes of the blades into account.*

Conclusion. *The developed model, which takes the flapping movements and flexes of the helicopter main rotor blades into ac-count, can be used to improve the ISAR algorithms that provide radar imaging of aerial vehicles.*

Key words: mathematical model, main rotor, helicopter, inverse synthetic-aperture radar

For citation: Heister S. R., Thai T. Nguyen. Mathematical models of the radar signal reflected from a helicopter main rotor in application to inverse synthesis of antenna aperture. Journal of the Russian Universities. Radioelectronics. 2019, vol. 22, no. 3, pp. 74–87. doi: 10.32603/1993-8985-2019-22-3-74-87

Acknowledgements. Initiative work.

Conflict of interest. Authors declare no conflict of interest.

Submitted 09.04.2019; accepted 20.05.2019; published online 27.06.2019

С. Р. Гейстер[1]✉, Т. Т. Нгуен[2]

*[1]ЗАО "Группа производственных технологий и авиационного машиностроения Аэромаш"
ул. Аэродромная, 3, п. Мачулищи Минского района, Республика Беларусь*

*[2]Белорусский государственный университет информатики и радиоэлектроники
ул. П. Бровки, 6, г. Минск, 220013, Республика Беларусь*

МАТЕМАТИЧЕСКИЕ МОДЕЛИ РАДИОЛОКАЦИОННОГО СИГНАЛА, ОТРАЖЕННОГО ОТ НЕСУЩЕГО ВИНТА ВЕРТОЛЕТА, В ПРИЛОЖЕНИИ К ОБРАЩЕННОМУ СИНТЕЗУ АПЕРТУРЫ

Аннотация.
Введение. *В основе решения задачи распознавания летательных аппаратов лежит формирование радиолокационных портретов, отражающих конструктивные особенности этих аппаратов. Высокой информативностью обладают портреты, представляющие собой радиолокационные изображения винтов летательных аппаратов. Они позволяют различать количество и взаимное расположение лопастей винта, а также направление его вращения. В основе получения таких изображений лежат математические модели отраженных сигналов.*
Цель работы. *Рассмотрение математических моделей сигнала, отраженного от винта вертолета, в приложении к обращенному синтезу апертуры антенны (ОСАА).*
Методы и материалы. *Обращенный синтез используется для построения радиолокационного изображения винта в радиолокационном датчике с монохроматическим зондирующим сигналом. Лопасти винта в моделях аппроксимируются разными геометрическими формами. Модели, используемые для описания отражений от винтов вертолетов и винтовых самолетов, имеют существенные отличия. В процессе перемещения каждая лопасть несущего винта вертолета совершает характерные движения (маховое движение, качание, закручивание), а также изгибается в вертикальной плоскости. Такие движения и изгибы лопастей оказывают влияние на фазовую структуру сигнала, отраженного от несущего винта. При разработке алгоритма построения изображения несущего винта на основе ОСАА необходимо максимально точно учесть закон изменения фазовой структуры отраженного сигнала.*
Результаты. *Установлено, что в сантиметровом диапазоне длин волн математическая модель сигнала, отраженного от несущего винта вертолета как системы лопастей, наиболее точно описывается представлением каждой лопасти набором изотропных отражателей, расположенных на передней и задней кромках лопасти. Учет маховых движений и изогнутых форм лопастей в модели сигнала, отраженного от винта вертолета, позволяет максимально приблизиться к особенностям реального сигнала.*
Заключение. *Разработанная модель, учитывающая маховые движения и изгибы лопастей несущего винта вертолета, может использоваться для совершенствования алгоритмов ОСАА, обеспечивающих построение радиолокационных изображений летательных аппаратов.*

Ключевые слова: математическая модель, несущий винт, вертолет, обращенный синтез апертуры антенны

Для цитирования: Гейстер С. Р., Нгуен Т. Т. Математические модели радиолокационного сигнала, отраженного от несущего винта вертолета, в приложении к обращенному синтезу апертуры // Изв. вузов России. Радиоэлектроника. 2019. Т. 22, № 3. С. 74–87. doi: 10.32603/1993-8985-2019-22-3-74-87

Источник финансирования. Инициативная работа.

Конфликт интересов. Авторы заявляют об отсутствии конфликта интересов.

Статья поступила в редакцию 09.04.2019; принята к публикации 20.05.2019; опубликована онлайн 27.06.2019

Introduction. Considered as an object of radar surveillance, the movements of a single-rotor helicopter's primary elements are complex, consisting not only the translational motion of the fuselage, but also of the translational-rotational motions of the main rotor (MR) and tail rotor, during which the angles of attack of their blades change. When developing Inverse Synthetic Aperture Radar (ISAR) algorithms for imaging the rotors of different helicopters, it is necessary to account for the laws describing changes in the phase shifts of signals reflected from the elements of each rotor. The most commonly-used mathematical model of reflected signals (RS) for MR, in which the blades are represented as cylinders [1], only partially meets this requirement. Therefore, in the present study we set out to develop mathematical models for signals reflected from helicopter main rotors differing in the form of their blades. In order to proceed with the modelling, it is assumed that an aircraft can be represented as a complex of reflectors [2] in the centimetre wavelength range of radio-waves with the overall signal reflected from it consisting in a superposition of signals reflected from each reflector.

Model of the temporal structure of a signal reflected from a helicopter's main rotor. A rectangular coordinate system $(0XYZ)$ is bounded with a radar sensor (RdS) (Fig. 1), with its origin coinciding with the centre of the RdS and axis $0X$ parallel to the helicopter velocity vector *v*. Fig. 1 shows notations: $C-$ the MR rotation centre with coordinates (x_C, y_C, z_C), where $z_C = h_C$ is the flight altitude and r_C is the distance from RdS to the centre *C*. The helicopter's MR (Fig. 2) is considered as a system of $N_{\text{b.rot}}$ blades having an angular spacing $\Delta\phi_{\text{rot}} = 2\pi/N_{\text{b.rot}}$, rotating clockwise (top view) with frequency F_{rot} in the plane parallel to *XOY*, and moving along the axis $0X$ with a constant velocity. Blades are numbered along the rotation direction: $n_{\text{b.rot}} = \overline{1, N_{\text{b.rot}}}$, starting from the blade with minimal positive angle relative to the axis $0X$.

Let us introduce the local rectangular coordinate system $CX_1Y_1Z_1$ with an origin in point *C*; axis CX_1 directed to the helicopter tail; axis CZ_1 coinciding with the MR axis of rotation and directed upward. The angular position of $n_{\text{b.rot}}$ th blade relative to the axis CX_1 at moment *t* could be determined using the angular spacing of the first blade $\phi_{\text{b1}}(t)$, which initial angular position ϕ_0 at the moment $t = 0$ is

$$\phi_{\text{b}n_{\text{b.rot}}}(t) = \phi_{\text{b1}}(t) + \Delta\phi_{\text{rot}}\left(n_{\text{b.rot}} - 1\right), \qquad (1)$$

where

$$\phi_{\text{b1}}(t) = 2\pi F_{\text{rot}} t + \phi_0,\ n_{\text{b.rot}} = \overline{1, N_{\text{b.rot}}}.$$

Defining $\Delta t = 1/\left(F_{\text{rot}} N_{\text{b.rot}}\right)$, we transform expression (1) into the form:

$$\phi_{\text{b}n_{\text{b.rot}}}(t) = 2\pi F_{\text{rot}} t + \left(n_{\text{b.rot}} - 1\right)2\pi/N_{\text{b.rot}} + \phi_0 = 2\pi F_{\text{rot}}\left[t + \left(n_{\text{b.rot}} - 1\right)\Delta t\right] + \phi_0. \qquad (2)$$

The signal reflected from the rotor is represented as a combination of signals reflected from point-isotropic reflectors located on the surfaces of $N_{\text{b.rot}}$ blades. In general, the mathematical RS model on an antenna output is described by the expression [3]–[6]:

$$u_{\text{RS}}(t) = \sum_{n_{\text{b.rot}}=1}^{N_{\text{b.rot}}} \sum_{n_{\text{ref}}=1}^{N_{\text{ref}}} \sum_{l=0}^{L-1} U_0\left[t - lT_{\text{rep}} - t_{\text{d},n_{\text{b.rot}},n_{\text{ref}}}(t)\right] \times E_{n_{\text{b.rot}},n_{\text{ref}}}(t) \times \exp\left\{i\left[\omega_0 t + \varphi_{n_{\text{b.rot}},n_{\text{ref}}}(t)\right]\right\}. \qquad (3)$$

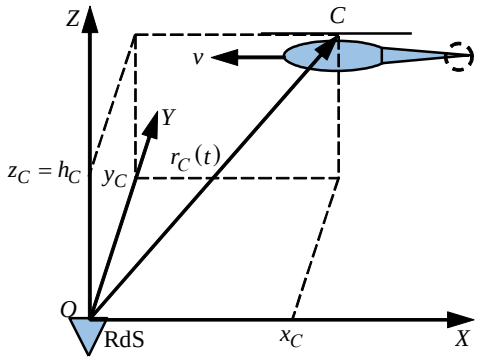

Fig. 1. Model of the helicopter's movement

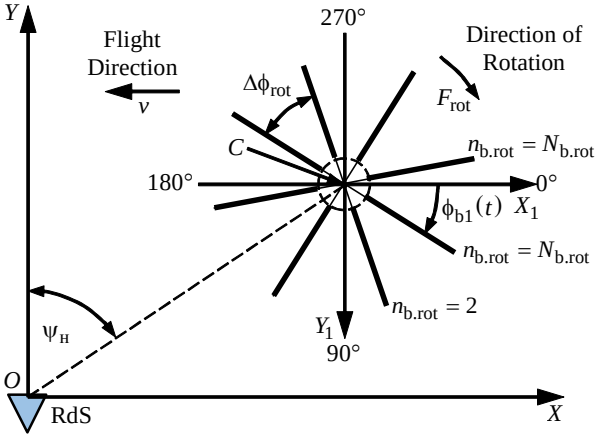

Fig. 2. Model of the helicopter's main rotor

where N_{ref} – the quantity of the reflectors on a single blade; $U_0(t)$ – the modulation law of a single probing signal (PS); L, T_{rep} – the quantity and the period of repetitions of the single signals in the emitting PS; $E_{n_{\text{b.rot}},n_{\text{ref}}}(t)$, $\varphi_{n_{\text{b.rot}},n_{\text{ref}}}(t)$, and $t_{\text{d},n_{\text{b.rot}},n_{\text{ref}}}(t)$ – the laws of change of the amplitude, phase and delay time of the signal reflected from n_{ref} th reflector on the $n_{\text{b.rot}}$ th blade, $\omega_0 = 2\pi f_0$ – the PS carrier frequency.

A complex RS envelope [3]–[6] in the case of a monochromatic probing signal (MCPS) is described by the expression:

$$U_{\text{b.rot}}(t) = \sum_{n_{\text{b.rot}}=1}^{N_{\text{b.rot}}} \sum_{n_{\text{ref}}=1}^{N_{\text{ref}}} E_{n_{\text{b.rot}},n_{\text{ref}}}(t) \exp\left\{ i\left[\varphi_{n_{\text{b.rot}},n_{\text{ref}}}(t) \right] \right\}. \quad (4)$$

The laws governing changes of amplitude, phase and delay time of a signal reflected from n_{ref} th reflector on the $n_{\text{b.rot}}$ th blade could be represented in the form:

$$\begin{gathered} E_{n_{\text{b.rot}},n_{\text{ref}}}(t) = \sqrt{2P_{\text{ref},n_{\text{b.rot}},n_{\text{ref}}}(t)}; \\ P_{\text{ref},n_{\text{b.rot}},n_{\text{ref}}}(t) = \frac{P_0 G_{\text{t}} G_{\text{r}} \lambda^2 \sigma_{n_{\text{b.rot}},n_{\text{ref}}}\left[\psi_{\text{H}}(t)\right]}{(4\pi)^3 r^4_{n_{\text{b.rot}},n_{\text{ref}}}(t)}; \\ \varphi_{n_{\text{b.rot}},n_{\text{ref}}}(t) = 2k r_{n_{\text{b.rot}},n_{\text{ref}}}(t); \\ t_{\text{d},n_{\text{b.rot}},n_{\text{ref}}}(t) = 2r_{n_{\text{b.rot}},n_{\text{ref}}}(t)/c, \end{gathered} \quad (5)$$

where $P_{\text{ref},n_{\text{b.rot}},n_{\text{ref}}}$ – the power of RS reflected from the n_{ref} th reflector on the $n_{\text{b.rot}}$ th blade; P_0 – the power of PS; G_{t}, G_{r} – the gain coefficients of the transmitter and receiver antennas, respectively; $\sigma_{n_{\text{b.rot}},n_{\text{ref}}}\left[\psi_{\text{H}}(t)\right]$ – the radar cross-section (RCS) of the n_{ref} th reflector on the $n_{\text{b.rot}}$ th blade at an angle $\psi_{\text{H}}(t)$; $r_{n_{\text{b.rot}},n_{\text{ref}}}$ – the distance to the n_{ref} th reflector on the $n_{\text{b.rot}}$ th blade; $k = 2\pi/\lambda$ – the wave number; λ and c – the wavelength and the velocity of PS propagation, relatively.

In order to ensure accurate radar imaging, it is necessary that the RS phase be represented correctly. Expressions (3)–(5) show that this phase is determined by the laws of change of the distances to the reflectors on the blades of the MR during rotation. The primary reflections from the MR are produced by the edges of its blades. Taking this into account, we will assume that the reflectors are placed not over the entire plane of the blade, but rather on its edges. Let us consider the laws of the change of the distances to the reflectors relative to the phase centre of RdS antenna for three options of the blade representation:

Option 1 – as a combination of isotropic reflectors located on a straight line whose length corresponds to the blade length;

Option 2 – as a combination of reflectors located on straight lines corresponding to the leading and the trailing edges of the blade;

Option 3 – as a combination of reflectors located on the lines, which is bent due to flapping and nonuniform blade bending. Blade feathering is not considered.

The reflectors on the edges of the blades are isotropic in the range of hemispheres directed toward RdS for Options 2 and 3.

It is worth mentioning that a helicopter moves according to the orientation and magnitude of the thrust force vector of the main rotor with respect to the gravity force vector. One may assume that the thrust force vector is oriented perpendicular to the plane of the base of the cone described by the moving main rotor blades except when the orientation of this plane is changed by a pilot using a swashplate. The reflected signal model, which takes the orientation of the blade system into account; its slope and form during horizontal flight with constant altitude relating to RdS is of interest in the application of radar imaging techniques for the main rotor.

The distance to the reflector in the case of blade representation according to Option 1. Reflectors are located (Fig. 3) in the range from $R_{\min}$ to $R_{\max}$ with a step of $\Delta R = \lambda/4$, therefore the reflector with the number n_{ref} is located in the distance of $R_{n_{\text{ref}}} = R_{\min} + (n_{\text{ref}} - 1)\Delta R$, $n_{\text{ref}} = \overline{1, N_{\text{ref}}}$ from the centre of rotation C.

At the beginning of the analysis, the centre of rota-

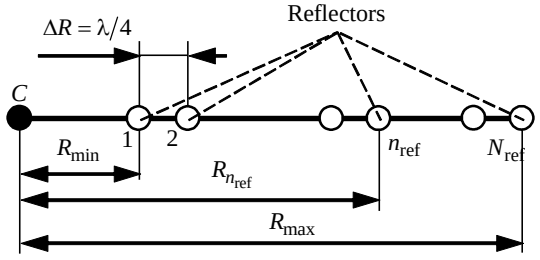

Fig. 3. Option 1 of the representation of the blade

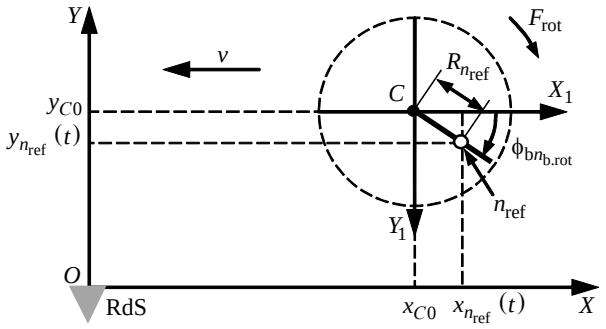

Fig. 4. Determination of the coordinates of the reflector for Option 1

tion is placed at the point having coordinates (x_{C0}, y_{C0}, z_{C0}) (Fig. 4). The flight velocity v of advancing to RdS helicopter is negative. The distance to the n_{ref} th reflector on the $n_{b.rot}$ th blade is determined by the expression:

$$r_{n_{b.rot},n_{ref}}(t) = \sqrt{z^2_{n_{b.rot},n_{ref}}(t) + y^2_{n_{b.rot},n_{ref}}(t) + x^2_{n_{b.rot},n_{ref}}(t)}, \quad (6)$$

where

$$x_{n_{b.rot},n_{ref}}(t) = x_{C0} + vt + R_{n_{ref}} \cos\left[\phi_{bn_{b.rot}}(t)\right];$$
$$y_{n_{b.rot},n_{ref}}(t) = y_{C0} - R_{n_{ref}} \sin\left[\phi_{bn_{b.rot}}(t)\right];$$
$$z_{n_{b.rot},n_{ref}}(t) = z_{C0}.$$

Distance to reflector in case of representation of the blade according to Option 2. Let us label reflectors on the leading and trailing edges by numbers $n_{ref.ld}$ and $n_{ref.tr}$ respectively $(n_{ref.ld} = n_{ref.tr} = \overline{1, N_{ref}})$ (Fig. 5). The distance from the reflector with number $n_{ref.ld}$ to the centre of rotation *C* is equal to $R_{n_{ref.ld}} = R_{min} + [n_{ref.ld} - 1]\Delta R$. The distance from the centre of rotation *C* to a projection of the reflector with number $n_{ref,tr}$ on the leading edge is calculated using the same formula. Coordinates $x_{n_{b.rot},n_{ref.ld}}(t)$, $y_{n_{b.rot},n_{ref.ld}}(t)$ and $z_{n_{b.rot},n_{ref.ld}}(t)$ of $n_{ref.ld}$ th reflector (Fig. 6) are determined by the expressions analogous

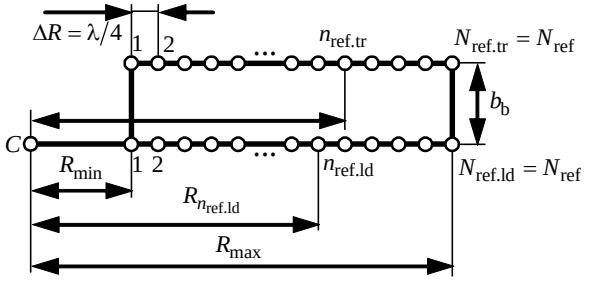

Fig. 5. Option 2 of the representation of the blade

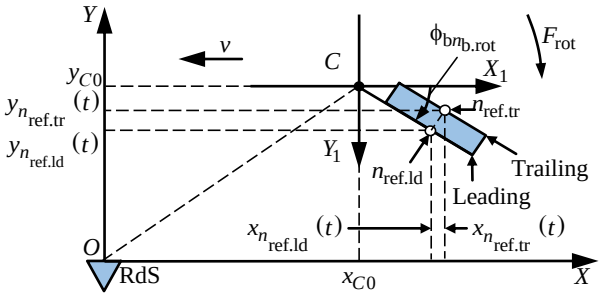

Fig. 6. Determination of the coordinates of the reflector for Option 2

to the expressions in (6). Coordinates of $n_{ref.tr}$ th reflector are determined by the expressions:

$$x_{n_{b.rot},n_{ref.tr}}(t) = x_{C0} + vt + R_{n_{ref.tr}} \cos\left[\phi_{bn_{b.rot}}(t)\right] + b_b \sin\left[\phi_{bn_{b.rot}}(t)\right];$$
$$y_{n_{b.rot},n_{ref.tr}}(t) = y_{C0} - R_{n_{ref.tr}} \sin\left[\phi_{bn_{b.rot}}(t)\right] + b_b \cos\left[\phi_{bn_{b.rot}}(t)\right];$$
$$z_{n_{b.rot},n_{ref.tr}}(t) = z_{C0},$$

where b_b – the blade chord.

The distance to the reflectors of the blade with respect to the change of reflection characteristics during advancing and retreating of the blades relating to RdS is described by the expressions:

$$r_{n_{b.rot},n_{ref.ld}}(t) = \sqrt{x^2_{n_{b.rot},n_{ref.ld}}(t) + y^2_{n_{b.rot},n_{ref.ld}}(t) + z^2_{n_{b.rot},n_{ref.ld}}(t)} \quad (7)$$

during advancing, and

$$r_{n_{b.rot},n_{ref.tr}}(t) = \sqrt{x^2_{n_{b.rot},n_{ref.tr}}(t) + y^2_{n_{b.rot},n_{ref.tr}}(t) + z^2_{n_{b.rot},n_{ref.tr}}(t)} \quad (8)$$

retreating.

An expression for the condition corresponding to the change of the reflecting edges during advancing (retreating) of the blades for clockwise rotation direction (top view) (see Fig. 2) is

– when

$$\pi/2 + \psi_H(t) \le \phi_{bn_{b.rot}}(t) \le 3\pi/4 + \psi_H(t)$$

the $n_{b.rot}$ th blade retreats from RdS and its trailing edge reflects;

– when

$$0 \le \phi_{bn_{b.rot}}(t) < \pi/2 + \psi_H(t) \text{ и}$$
$$3\pi/4 + \psi_H(t) < \phi_{bn_{b.rot}}(t) \le 2\pi$$

this blade advances to RdS and its leading edge reflects.

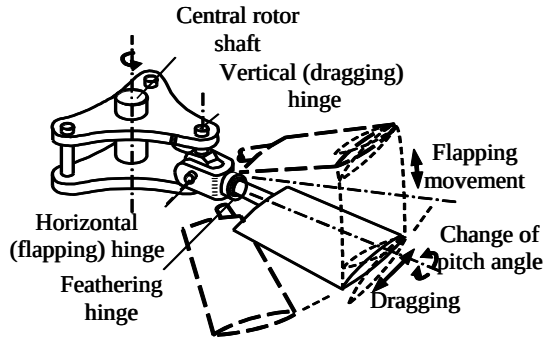

Fig. 7. **The main rotor mount and the blades movements**

The distance to the reflector in the case of representation of the blade according to Option 3. The main rotor of the helicopter creates a lifting force and a horizontal thrust force. In general, each MR blade is installed on the central rotor head by a horizontal (flapping) hinge (FH), a vertical (drag hinge (DH) and a feathering hinge (FrH), with respect to which flapping movements (FM), dragging (lead-lag) and feathering (change of pitch angles) are carried out (Fig. 7) [7]–[10].

A blade flapping angle reaches the values of 12–15° that leads to the end of the blade being lifted to a sufficient height with respect to the rotation plane of the rotor head and influences the RS phase in centi-metre range. In addition, the free end of the blade bends in the vertical plane during rotation of the MR leading to a change of the backscattering diagram and the phase of refractions from the edges*.

Description of the flapping movement and features of blade construction. We will assume for simplification that the helicopter is oriented horizontally during the flight and that the rotation plane of the rotor shaft is parallel to the Earth's surface at the point at which the helicopter is located. With respect to this, a coordinate system $CX_1Y_1Z_1$ (Fig. 8), whose centre is the rotational centre of the rotor, is used for describing FM. Axis CX_1 is in the rotation plane of the rotor head parallel to the axis $0X$ and directed toward the helicopter tail; axis CZ_1 is directed along the upward vertical axis. The position of the blade on the rotation plane is determined by angle ϕ_b; flapping angle β_b; blade section setup angle θ_b; shift of the flap hinge from the rotor shaft axis e_b.

It is worth mentioning that the angle of the blade section setup is the pitch angle of the blade cross-section chord relative to the rotation plane, which is perpendicular to the propeller rotation axis.

The flapping angle and pitch angle of the blade in a stationary state of flight comprises the periodic functions of its angular position ϕ_b. Therefore, this can be expanded in a Fourier series with respect to this parameter [7], [8], [11]:

$$\beta_b(\phi_b) = \beta_0 - \beta_{1c}\cos(\phi_b) - \beta_{1s}\sin(\phi_b) - \ldots - \\ -\beta_{mc}\cos(n\phi_b) - \beta_{ms}\sin(n\phi_b) - \ldots;$$
$$\theta_b(\phi_b) = \theta_0 - \theta_{1c}\cos(\phi_b) - \theta_{1s}\sin(\phi_b) - \ldots - \\ -\theta_{mc}\cos(n\phi_b) + \theta_{ms}\sin(n\phi_b) - \ldots,$$

where $\beta_0 = \overline{\beta_b(\phi_b)}$ – the coning angle, determined by the average value of the flapping angle β_b; β_{mc}, β_{ms}, $m = 1, 2, \ldots$ – the Fourier-harmonics for the flapping angle; θ_0 – the common step of the pitch angle; θ_{mc}, θ_{ms} – the Fourier-harmonics for the pitch angle.

In general, one should use only the first harmonics for description of this movements [7]–[14]:

$$\beta_b(\phi_b) = \beta_0 - \beta_{1c}\cos(\phi_b) - \beta_{1s}\sin(\phi_b);$$
$$\theta_b(\phi_b) = \theta_0 - \theta_{1c}\cos(\phi_b) - \theta_{1s}\sin(\phi_b).$$

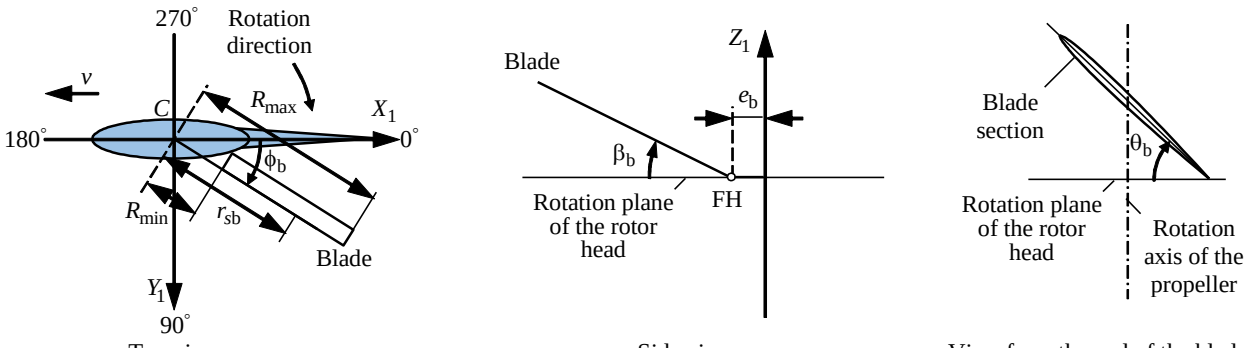

Fig. 8. Flapping motion of the blade

* By the phase structure of the signal reflected from the blade edge is meant a distribution of phases of the signals reflected from the edge fragments.

It is shown by the authors of this paper that influence of the pitch angle θ_b on the RS phase is very low, thus, let us consider only flapping angle β_b. Coefficients of the flapping angle β_b expansion are determined according to the equilibrium conditions of the inertial moments, centrifugal moment and aerodynamic forces of the blade relative to FH. It is possible to obtain the equation of blade flapping oscillations relative to FH from the equation of the moment's equilibrium [7], [8], [11]:

$$J_F \frac{d^2\beta_b\left[\phi_b(t)\right]}{dt^2} + J_b\omega_{rot}^2\upsilon^2\beta_b\left[\phi_b(t)\right] = \int_0^{R_{max}} T\left[r_{sb},\ \phi_b(t)\right] r_{sb}\, dr_{sb}, \quad (9)$$

where J_F – the mass inertia moment of the blade relative to FH; $\omega_{rot} = 2\pi F_{rot}$ – the angular velocity of the propeller rotation; $\upsilon = \sqrt{1+(S_F e_b)/J_F}$ – the nondimensional frequency of the blade flapping self-oscillations relative to FH; R_{max} – the main rotor radius; $T\left[r_{sb},\ \phi_b(t)\right]$ – the blade aerodynamic force per unit length; r_{sb} – the radius of the analysis point, and S_F – the static moment of the blade relative to FH.

Solving equation (9) is complicated task. In the considered case, one could use the results obtained in the paper [11] assuming that a feathered blade is in the rectangular form, while a flapping controller is absent and the distribution of inductive velocities along the sweep away disk is uniform.

For these conditions:

$$\beta_0 = \frac{\gamma}{\upsilon^2}\left[\frac{1}{4}\theta_0\left(1+\mu_{rot}^2\right) + \frac{1}{3}\lambda_{rot} - \frac{1}{3}\mu_{rot}\theta_{1s}\right];$$

$$\beta_{1c} = \frac{\frac{1}{8}\gamma^2\mu_{rot}\left(1+\frac{\mu_{rot}^2}{2}\right)\left(\lambda_{rot}+\frac{4}{3}\theta_0-\theta_{1s}\mu_{rot}\right)}{\frac{1}{16}\gamma^2\left(1-\frac{\mu_{rot}^4}{4}\right)+\left(\upsilon^2-1\right)^2} - \frac{\frac{1}{16}\gamma^2\left(1-\frac{\mu_{rot}^4}{4}\right)\theta_{1s}}{\frac{1}{16}\gamma^2\left(1-\frac{\mu_{rot}^4}{4}\right)+\left(\upsilon^2-1\right)^2} + \frac{\gamma\left[\frac{1}{3}\mu_{rot}\beta_0+\frac{1}{4}\theta_{1c}\left(1+\frac{\mu_{rot}^2}{2}\right)\right]\left(\upsilon^2-1\right)}{\frac{1}{16}\gamma^2\left(1-\frac{\mu_{rot}^4}{4}\right)+\left(\upsilon^2-1\right)^2};$$

$$\beta_{1s} = \frac{\frac{1}{4}\gamma^2\left(1-\frac{\mu_{rot}^2}{2}\right)\left(\frac{1}{3}\beta_0\mu_{rot}\right)}{\frac{1}{16}\gamma^2\left(1-\frac{\mu_{rot}^4}{4}\right)+\left(\upsilon^2-1\right)^2} + \frac{\frac{1}{16}\gamma^2\left(1-\frac{\mu_{rot}^4}{4}\right)\theta_{1c}}{\frac{1}{16}\gamma^2\left(1-\frac{\mu_{rot}^4}{4}\right)+\left(\upsilon^2-1\right)^2} - \frac{\gamma\left[\left(\frac{1}{2}\lambda_{rot}+\frac{2}{3}\theta_0\right)\mu_{rot}-\theta_{1s}\left(\frac{1}{4}+\frac{3}{8}\mu_{rot}^2\right)\right]\left(\upsilon^2-1\right)}{\frac{1}{16}\gamma^2\left(1-\frac{\mu_{rot}^4}{4}\right)+\left(\upsilon^2-1\right)^2},$$

where

$$\gamma = \frac{b_b\rho\alpha_\infty R_{max}^4}{2J_F}$$

– the blade mass characteristic;

$$\mu_{rot} = \frac{v\cos(\alpha_{rot})}{\omega_{rot}R_{max}}$$

– the flight regime characteristic;

$$\lambda_{rot} = \frac{v\sin(\alpha_{rot})+\upsilon_1}{\omega_{rot}R_{max}},$$

– the flow characteristic, and ρ – the air mass density; α_∞ – the derivative of the lifting force coefficient in the blade section with respect to the setup angle; α_{rot} – the incidence angle of the propeller rotation plane (the cone base plane) relative to the horizontal plane; υ_1 – inductive flow velocity.

An alteration in the general step of the pitch angle θ_0 using the swashplate (SP) leads to a change in the lifting force and, consequently, to a change of the coning angle β_0. The change of the cyclic step of the pitch angle θ_{1c} by deviation of the SP plate forward or backward (in pitch) leads to a change of the incidence angle of the cone base β_{1c}. An analogous change of the cyclic step of pitch angle θ_{1s} to the right or to the left (in roll) leads to a change of the incidence angle β_{1s}.

The MR blades have the following construction features. The base of the blade is a longeron forming a leading part of the blade profile. The trailing part is attached to this longeron. All-metal blades could be divided into two groups: (1) – with a tube steel longe-

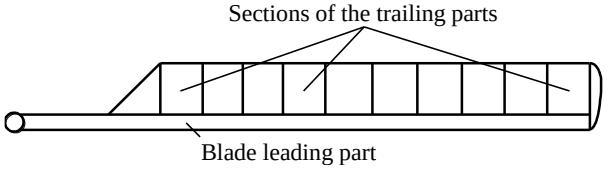

Fig. 9. Blade design features

ron (Mi-6 and Mi-26), and (2) – with a extruded light alloy longeron (Mi-2, Mi-8, Mi-24) [12]–[14]. The trailing part of the blade is made in form of a split construction for decrease the influence of a variable strains, and usually consists of sections, which are not bounded rigidly. These sections are based on cellular structures with rubber inserts between them (Fig. 9) [12]–[14]. In the case of longeron deformation the trailing part is not stressed. Use of separate sections in the blade construction allows the blade to be feathered and the relevant section to be replaced in the case of damage [12]–[14].

Model of the signal reflected from the main rotor with respect to the flapping movements and bends. The rectangular coordinate system $0XYZ$ is used during the simulation (see Fig. 1). The edges of the main rotor are represented as a set of reflectors placed on the edge lines. Leading and trailing edges are described by a piecewise linear function within this model. For example, the leading edge of the main rotor of the Mi-2 helicopter is approximated (Fig. 10, *a*) by two sections whose lengths are R_{ld1} and R_{ld2}, respectively; the incidence angle of the second section relative to the first section is β_{ld2}; the trailing edge (Fig. 10, *b*) is approximated by four sections, whose lengths are R_{tr1}, R_{tr2}, R_{tr3}, R_{tr4}, respectively, while the incidence angles of the second, third, and fourth sections relative to the first section are β_{tr2}, β_{tr3}, β_{tr4}, respectively. The incidence angle of the first approximation section of leading and trailing edges corresponds to the current flapping angle $\beta_{\text{b}}(\phi_{\text{b}})$.

Let us define the distance from the center of rotation C to the $n_{\text{ref.ld}}$ th reflector as $R_{n_{\text{ref.ld}}}$, and the distance from the centre of rotation to the projection of $n_{\text{ref.tr}}$ th reflector on the leading edge as $R_{n_{\text{ref.tr}}}$. Projections of these distances on the rotation plane of the rotor head is defined as $R_{\text{p},n_{\text{ref,ld}}}$ and $R_{\text{p},n_{\text{ref.tr}}}$, respectively (Fig. 10). Let us assume that the reflectors are placed on the edges at regular intervals ΔR. The quantity of the reflectors on the sections is determined by the rounding function:

$$N_{\text{ld}\varsigma} = \text{ceil}\left[R_{\text{ld}\varsigma}/\Delta R\right];\ \varsigma = 1,\ 2;$$
$$N_{\text{tr}\xi} = \text{ceil}\left[R_{\text{tr}\xi}/\Delta R\right];\ \xi = \overline{1,\ 4};$$
$$N_{\text{ref}} = \sum_{\varsigma=1}^{2} N_{\text{ld}\varsigma} = \sum_{\xi=1}^{4} N_{\text{ld}\xi}.$$

Projections $R_{\text{p},n_{\text{ref.ld}}}$ and $R_{\text{p},n_{\text{ref.tr}}}$ is the functions of ϕ_{b}, because β_{b} is the function of the ϕ_{b}. These projections are calculated using of $R_{n_{\text{ref.ld}}}$, $R_{n_{\text{ref.tr}}}$ and the incidence angles of the linear sections.

The angular position could be represented as a time function $\phi_{\text{b1}}(t) = \omega_{\text{rot}} t + \phi_0$. Let us assume that the helicopter is moving to the RdS along the trajectory parallel to axis $0X$ with constant velocity v at fixed height (see Fig. 1). The laws of change of the coordinates of the $n_{\text{ref.ld}}$ th reflector is described by the expressions:

$$x_{n_{\text{ref.ld}}}(t) = $$
$$= x_{C0} + vt + R_{\text{p},n_{\text{ref.ld}}}\left[\phi_{\text{b1}}(t)\right]\cos\left[\phi_{\text{b1}}(t)\right];$$
$$y_{n_{\text{ref.ld}}}(t) = $$
$$= y_{C0} - R_{\text{p},n_{\text{ref.ld}}}\left[\phi_{\text{b1}}(t)\right]\sin\left[\phi_{\text{b1}}(t)\right];$$

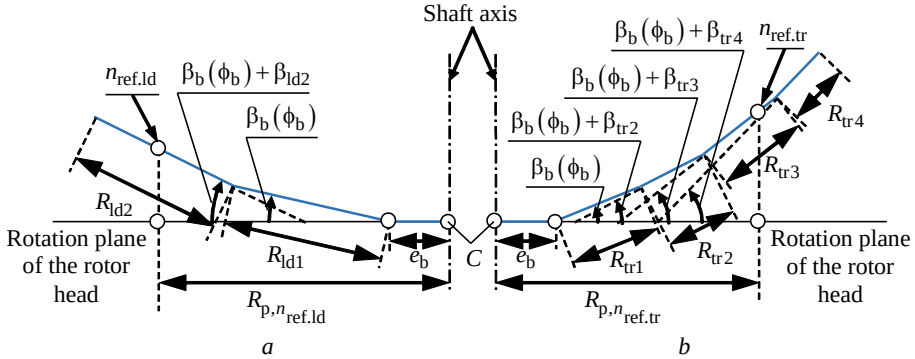

Fig. 10. Approximation of the rotor blade edges: *a* – the leading edge; *b* – the trailing edge

$$z_{n_{\text{ref.ld}}}(t) = \begin{cases} z_{C0} + (n_{\text{ref.ld}} - 1)\Delta R \sin\{\beta_{\text{b}}[\phi_{\text{b1}}(t)]\}, \\ \qquad 1 \le n_{\text{ref.ld}} \le N_{\text{ld1}}; \\ z_{C0} + R_{\text{ld1}} \sin\{\beta_{\text{b}}[\phi_{\text{b1}}(t)]\} + \\ + (n_{\text{ref.ld}} - N_{\text{ld1}} - 1)\Delta R \sin\{\beta_{\text{b}}[\phi_{\text{b1}}(t)] + \beta_{\text{ld2}}\}, \\ \qquad N_{\text{ld1}} < n_{\text{ref.ld}} \le N_{\text{ref}}, \end{cases} \quad (10)$$

and coordinates of the $n_{\text{ref.tr}}$ th reflector by the expressions:

$$x_{n_{\text{ref.tr}}}(t) = x_{C0} + vt + \\ + R_{\text{p},n_{\text{ref.tr}}}[\phi_{\text{b1}}(t)]\cos[\phi_{\text{b1}}(t)] + b_{\text{b}} \sin[\phi_{\text{b1}}(t)];$$

$$y_{n_{\text{ref.tr}}}(t) = y_{C0} - \\ - R_{\text{p},n_{\text{ref.tr}}}[\phi_{\text{b1}}(t)]\sin[\phi_{\text{b1}}(t)] + b_{\text{b}} \cos[\phi_{\text{b1}}(t)];$$

$$z_{n_{\text{ref.tr}}}(t) = \begin{cases} z_{C0} + (n_{\text{ref.tr}} - 1)\Delta R \sin\{\beta_{\text{b}}[\phi_{\text{b1}}(t)]\}, \\ \qquad 1 \le n_{\text{ref.tr}} \le N_{\text{tr1}}; \\ z_{C0} + R_{\text{tr1}} \sin\{\beta_{\text{b}}[\phi_{\text{b1}}(t)]\} + \\ + (n_{\text{ref.tr}} - N_{\text{tr1}} - 1)\Delta R \sin\{\beta_{\text{b}}[\phi_{\text{b1}}(t)] + \beta_{\text{tr2}}\}, \\ \qquad N_{\text{tr1}} < n_{\text{ref.tr}} \le N_{\text{tr1}} + N_{\text{tr2}}; \\ z_{C0} + R_{\text{tr1}} \sin\{\beta_{\text{b}}[\phi_{\text{b1}}(t)]\} + \\ + R_{\text{tr2}} \sin\{\beta_{\text{b}}[\phi_{\text{b1}}(t)] + \beta_{\text{tr2}}\} + \\ + (n_{\text{ref.tr}} - N_{\text{tr1}} - N_{\text{tr2}} - 1) \times \\ \times \Delta R \sin\{\beta_{\text{b}}[\phi_{\text{b1}}(t)] + \beta_{\text{tr3}}\}, \\ \qquad N_{\text{tr1}} + N_{\text{tr2}} < n_{\text{ref.tr}} \le N_{\text{tr1}} + N_{\text{tr2}} + N_{\text{tr3}}; \\ z_{C0} + R_{\text{tr1}} \sin\{\beta_{\text{b}}[\phi_{\text{b1}}(t)]\} + \\ + R_{\text{tr2}} \sin\{\beta_{\text{b}}[\phi_{\text{b1}}(t)] + \beta_{\text{tr2}}\} + \\ + R_{\text{tr3}} \sin\{\beta_{\text{b}}[\phi_{\text{b1}}(t)] + \beta_{\text{tr3}}\} + \\ + (n_{\text{ref.tr}} - N_{\text{tr1}} - N_{\text{tr2}} - N_{\text{tr3}} - 1) \times \\ \times \Delta R \sin\{\beta_{\text{b}}[\phi_{\text{b1}}(t)] + \beta_{\text{tr4}}\}, \\ \qquad N_{\text{tr1}} + N_{\text{tr2}} + N_{\text{tr3}} < n_{\text{ref.tr}} \le N_{\text{ref}}. \end{cases} \quad (11)$$

It is worth mentioning that flight velocity v is negative during the helicopter's advancement to RdS and positive during retreat.

The distance to an arbitrary reflector with respect to the change of reflecting edges of the first blade during its advancing and retreating is described by the general expressions (7), (8) using new coordinates (10), (11) and substituting the angular position of the first blade by the angular position of the $n_{\text{b.rot}}$ th blade, which is derived using expressions (1) and (2). The change condition of the edges' reflecting characteristics remains the same.

Simulation results for the main rotor of a Mi-2 helicopter. The following variable values were used during the simulation: rotation frequency of the propeller $F_{\text{rot}} = 4.119$ Hz; number of blades $N_{\text{b.rot}} = 3$; blade radius $R_{\max} = 7.25$ m, $R_{\min} = 0.9$ m; blade chord $b_{\text{b}} = 0.4$ m; initial coordinates of the rotor centre $x_{C0} = 206.8$ m, $y_{C0} = 209.2$ m, $z_{C0} = 52.8$ m; flight velocity $v = 7$ m/s; initial angular position of the first blade $\phi_0 = 30°$; $\lambda = 1.25 \cdot 10^{-2}$ m; probing signal – MCPS, ADC sampling rate $F_{\text{S}} = 96$ kHz. All reflectors are isotropic within the approximation region.

The RS power for the leading edge is higher than the power for the trailing edge in the case of a helicopter moving away, and vice versa [15]–[18]. Thus, the RCS of the single reflector of the leading edge for Options 1–3 is set to be $\sigma_{n_{\text{b.rot}},n_{\text{ref.ld}}}(t) = 4.5 \cdot 10^{-3}\,\text{m}^2$, while the RCS of the single reflector of the trailing edge for Options 2, 3 is set to be $\sigma_{n_{\text{b.rot}},n_{\text{ref.tr}}}(t) = 5 \cdot 10^{-3}\ \text{m}^2$. The lengths and the incidence angles of sections are $R_{\text{ld1}} = R_{\text{ld2}} = 0.5(R_{\max} - R_{\min})$; $\beta_{\text{ld2}} = 4.5°$; $R_{\text{tr1}} = R_{\text{tr2}} = R_{\text{tr3}} = R_{\text{tr4}} = 0.25(R_{\max} - R_{\min})$; $\beta_{\text{tr2}} = 2.5°$; $\beta_{\text{tr3}} = 4.5°$; $\beta_{\text{tr4}} = 6.5°$. Empirical data on a Mi-2 helicopter presented in [9], [10] was used for calculating the flapping movement coefficients: the blade mass characteristic $\gamma = 0.762$; the blade inertial moment relating to FH $J_{\text{b}} = 804\ \text{kg} \cdot \text{m}^2$; the blade static moment relating to FH $S_{\text{b}} = 197\ \text{kg} \cdot \text{m}$; the FH shift $e_{\text{b}} = 0.102$ m; the incidence angle of the main rotor rotation plane relating to the horizontal plane $\alpha_{\text{rot}} = 5°$; the inductive flow velocity $\upsilon_1 \cong 9$ m/s; the pitch angle steps $\theta_0 = 7°$, $\theta_{1\text{c}} = 5.73°$, $\theta_{1\text{s}} = 0°$.

The simulation results in the blade approximation according to Option 1 are shown on Fig. 11: *a* – real part of RS $\text{Re}U_{\text{b.rot}}$, *b* – the fragment of this signal – two pulses of RS, *c* – RS for the advancing blade, *d* – RS for retreating blade, *e* – energy spectrum of RS *S*, and *f* – its fragment*.

Simulation results in the blade approximation according to Option 2. Fig. 12 shows: *a* – real part of RS, *b* – the energy spectrum of RS, *c* – RS for the advancing blade, and *d* – RS for the retreating blade.

Simulation results in the blade approximation according to Option 3. Fig. 13 shows the dependence of the flapping angle on the blade's angular position for

* f_{D} – the Doppler frequency of the RS reflected from MR.

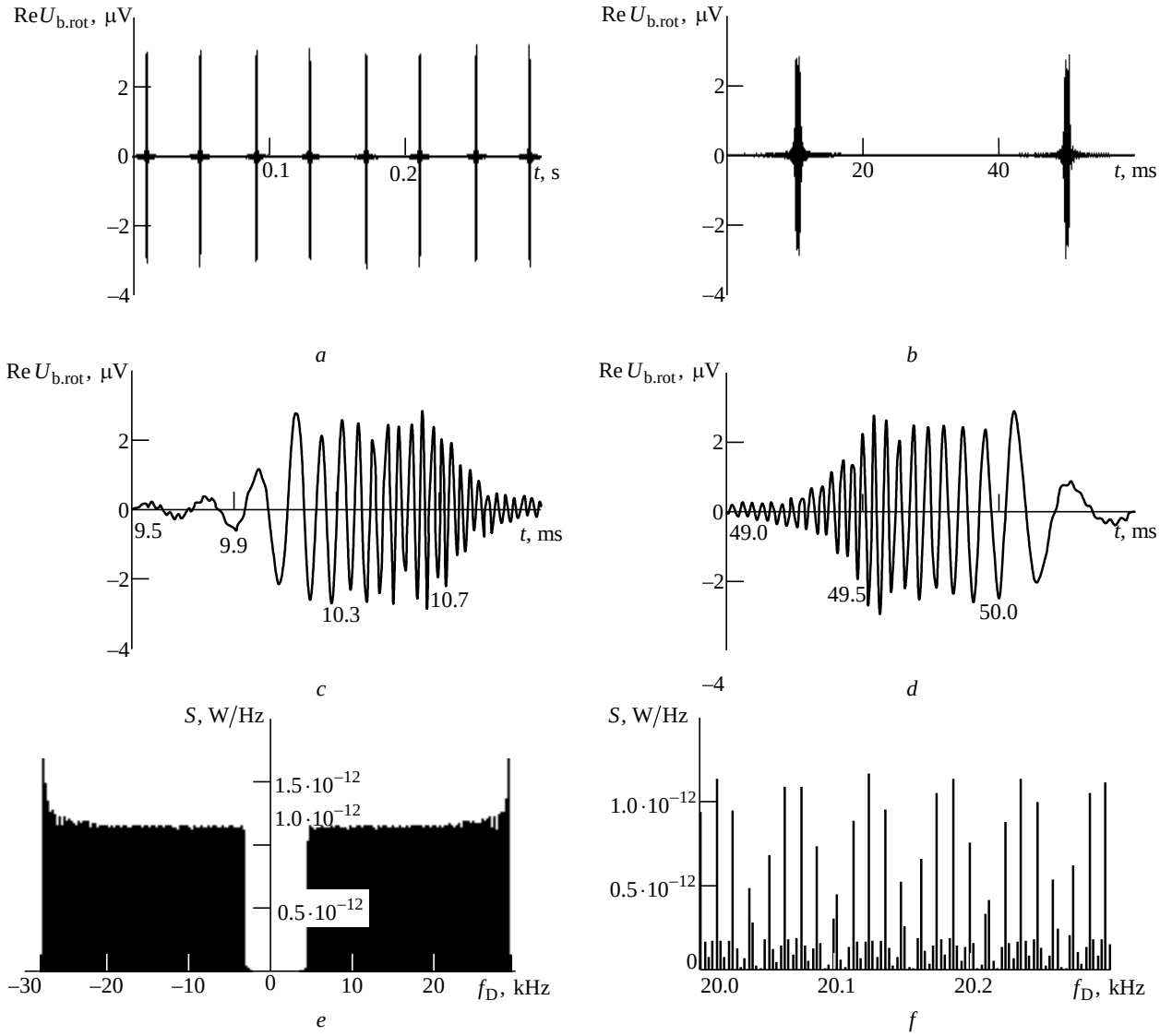

Fig. 11. Simulation results in the approximation according to Option 1:
Reflected signals: *a* – from the main rotor; *b* – from the main rotor (fragment); *c* – from the approaching blade; *d* – from the retreating blade. Energy spectrum: *e* – full; *f* – fragment

different flight velocities. Fig. 14 shows the simulation results: *a* – real part of RS, *b* – the energy spectrum of RS taking into account flapping movements and blade bending at flight velocity 7 m/s, *c* – RS for an advancing blade, *d* – RS for a retreating blade.

Analysis of the simulation results. RS for multiblade structure of MR comprises a set of pulses with frequency modulation. Each RS pulse consists of the chirp pulses adjacent to each other in the case of the piecewise linear approximation according to Option 3. Its quantity and modulation parameters are defined by the quantity of linear sections, their position on the edge, and propeller rotation frequency. RS pulse frequency is defined by multiplication of the blade quantity and the rotation frequency $N_{b.rot}F_{rot}$ of the propeller (see Fig. 11, *a*; 12, *a*; 14, *a*). The spectrum structure of the signal reflected from the MR is discrete (see Fig. 11, *f*). Spectrum components are divided by the intervals $N_{b.rot}F_{rot}$. Peaks in the RS spectrum observed during simulation for approximation according to Option 3 (see Fig. 14, *b*) are caused by a longer accumulation of the reflected signals in the area of blade backscattering diagram sidelobe. Analogue peaks present in the RS spectra obtained during the experimental investigation are additionally represented.

Results of the experimental investigation for a Mi-2 helicopter. The experimental conditions were as follows: the hovering helicopter slowly moves sideways to the RdS at a distance range from 40 to 30 m at a height of 3 m. Probing signal is MCPS with circular polarisation and $\lambda = 0.0125$ m. The RS sampling rate

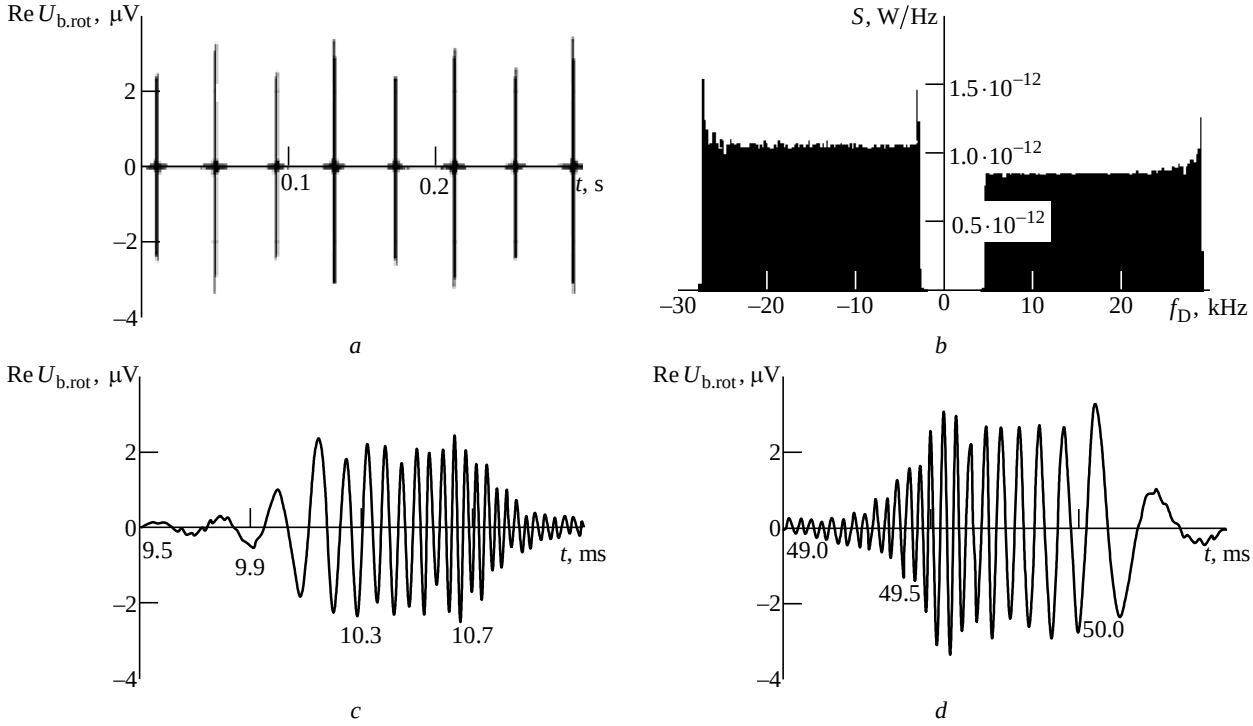

Fig. 12. Simulation results in the approximation according to Option 2:
a – the reflected signal from the main rotor; *b* – energy spectrum of the reflected signal;
c – reflected signal from the approaching blade; *d* – reflected signal from the retreating blade

is 48 kHz. Fig. 15 shows the results of investigation of the signal reflected from MR after compensation of the signal reflected from the helicopter body and the disturbing reflections. Coherent accumulation time (spectrum formation) $T_a = 1.365$ s.

The figures show the real part of RS for MR (*a* – general view, *b* – fragment), RS for advancing (*c*) and retreating blades (*d*), the energy spectrum of MR RS (*e* – general view, *f* – fragment).

Correlation of results. A comparison of the simulation data and the experimental results shows that the RS model of the helicopter MR, which takes into account the flapping movements and the bended blade forms, is close to the real RS. Each pulse of the RS complex envelope (see Fig. 14, *c* and *d*; 15, *c* and *d*) consists of short pulses adjacent to each other. The quantity, duration and modulation parameters of these pulses are determined by the quantity, position, and orientation of linear sections on the corresponding edge. In particular, RS of the leading edge of the Mi-2 helicopter rotor consists of two pulses (see Fig. 14, *c*) during its advancement to RdS, while the RS of the trailing edge during its retreat from RdS consists of four partial pulses (see Fig. 14, *d*). The partial pulse duration is determined by the backscattering diagram sidelobe from the corresponding linear section of the blade edge (see Fig. 11, *c* and *d*; 12, *c* and *d*; Fig. 14, *c* and *d;* 15, *c* and *d*). Since the spectra of the signals reflected from advancing and retreating blades are placed symmetrically relative to the Doppler frequency signal reflected from the helicopter body, they have different levels (Fig. 12, *b*; 14, *b*; 15, *e*).

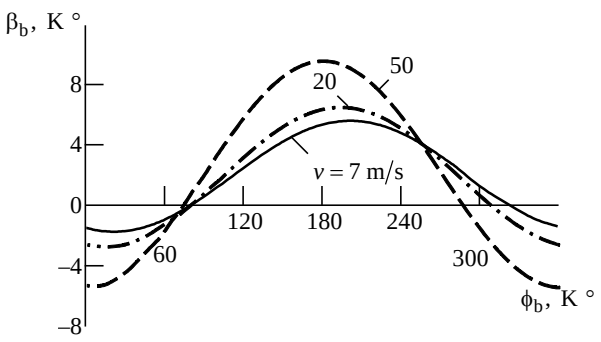

Fig. 13. The dependence of the flapping angle on the angular position of the blade (approximation according to option 3)

Conclusion. In the centimetre wavelength range, the mathematical model of the signal reflected from the main rotor considered as a system of the blades is described most precisely by representing of each blade as a set of isotropic reflectors located on leading and trailing blade edges. Taking the flapping movements and the bended forms of the blades into account allows the actual signal features to be maximally approximated, describing the signal phase structural change law more precisely, and, consequently, increasing the quality of the propeller radar imaging. The developed model could be used for improving the ISAR algorithms used to support the radar imaging.

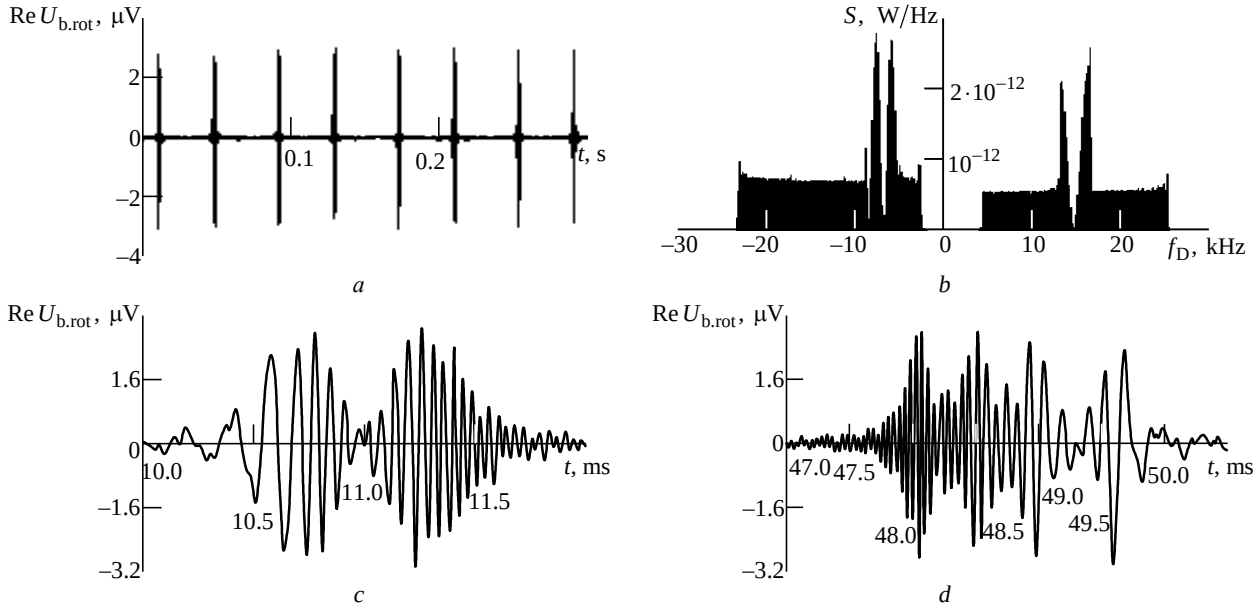

Fig. 14. Simulation results in the approximation according to Option 3:
a – the reflected signal from the main rotor; *b* – energy spectrum of the reflected signal;
c – reflected signal from the approaching blade; *d* – reflected signal from the retreating blade

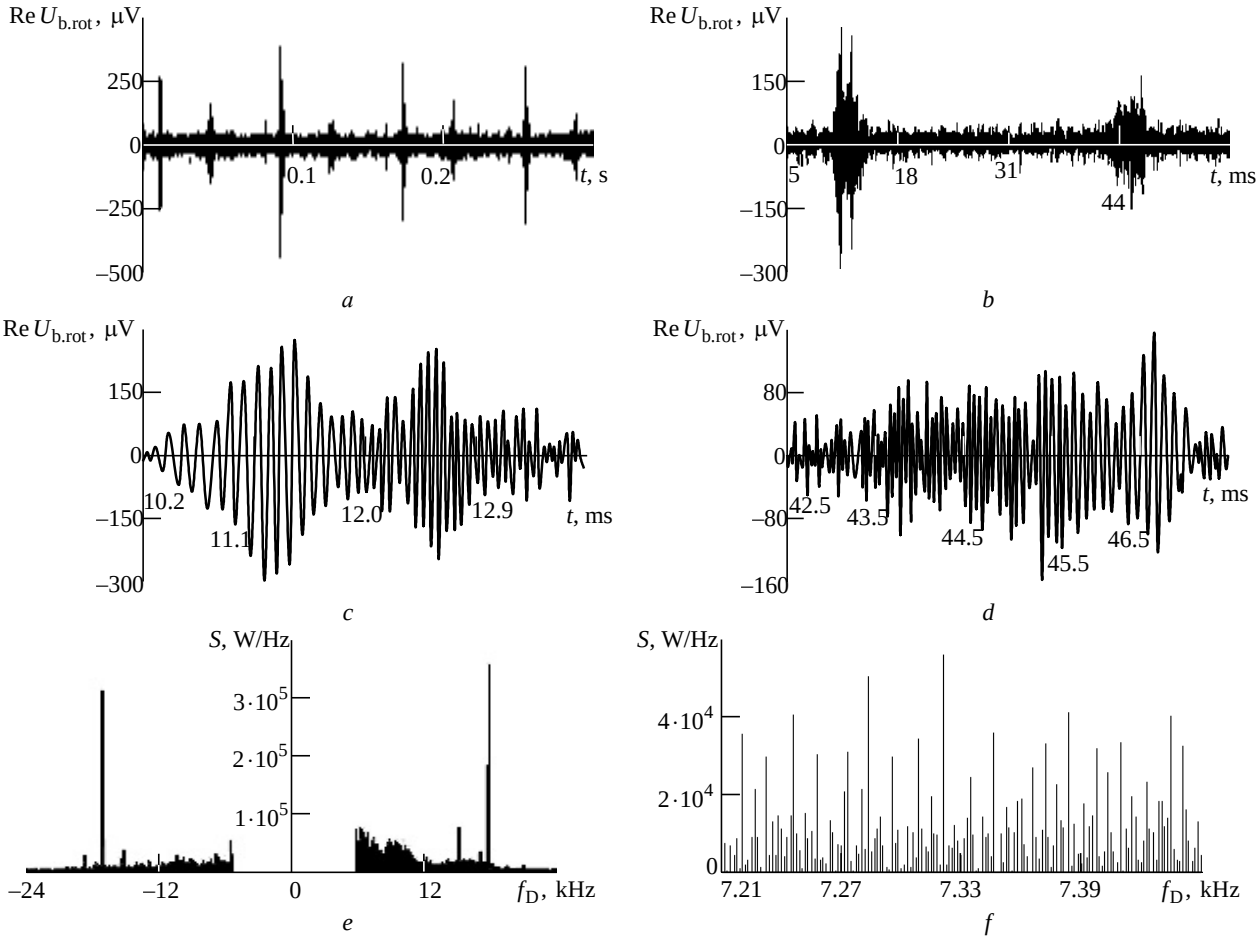

Fig. 15. Experimental results
Reflected signals: *a* – from the main rotor; *b* – from the main rotor (fragment); *c* – from the approaching blade;
d – from the retreating blade. Energy spectrum: *e* – full; *f* – fragment

REFERENCES

1. Vasil'yev O. V., Kutakhov P. V., Shchekotilov V. G., Yurchik I. A. Experimental Validation of the Model of a Radar Signal Reflected from a Helicopter. Radiotekhnika, 2001, no. 11, pp. 12–16. (In Russ.)

2. Varganov M. E., Zinov'yev Yu. S., Astanin L. Yu., Kostylev A. A., Pasmurov A. Ya., Sarychev V. A., Slezkinskii S. K., Dmitriev B. D. *Radiolokatsionnyye kharakteristiki letatel'nykh apparatov* [Radar Characteristics of Airborne Vehicles], ed. by L. T. Tuchkova. Moscow, *Radio i svyaz'*, 1985, 235 p. (In Russ.)

3. Barton D. K. Radar system analysis. Englewood Cliffs, NJ, Prentice Hall, 1964.

4. Shirman Ya. D., Losev Yu. I., MInervin N. N., Moskvitin S. V., Gorshkov S. A., Lekhovitskii D. I., Levchenko L. S. *Radioelektronnyye sistemy: Osnovy postroyeniya i teoriya* [Radio Electronic Systems. Basics of Construction and Theory], ed. by Ya. D. Shirman. Moscow, *ZAO "MAKVIS"*, 1998, 828 p. (In Russ.)

5. Bakulev P. A. *Radiolokatsiya dvizhushchikhsya tseley* [Radar Detection of Moving Targets]. Moscow, *Sovetskoye radio*, 1964, 336 p. (In Russ.)

6. Radar handbook: ed by M. I. Skolnik. In 4 vol. Vol. 1. New York, McGraw-Hill, Technology & Engineering, 1970.

7. Johnson W. Helicopter Theory. Princeton, Princeton University Press, 1980.

8. Yur'yev B. N. *Izbrannyye trudy. Tom 1. Vozdushnyye vinty, vertolety* [Propellers. Helicopters]. Moscow, *Izdatel'stvo akademii nauk SSSR,* 1961, 553 p. (In Russ.)

9. Zozulya V. B., Laletin K. N., Guchenko N. I. *Prakticheskaya aerodinamika vertoleta Mi-2* [Practical Aerodynamics of the Mi-2 Helicopter]. Moscow, *Vozdushnyy transport*, 1984, 176 p. (In Russ.)

10. Romanchuk V. N., Krasil'nikov V. V. *Vertolet Mi-2* [Mi-2 Helicopter]. Moscow, Transport, 1972, 260 p. (In Russ.)

11. Borisov E. A., Leont'yev V. A., Novak V. N. *Analiz osobennostey raboty nesushchego vinta s otritsatel'nym vynosom gorizontal'nykh sharnirov* [Analysis of the Features of the Rotor with a Negative Removal of Horizontal Hinges]. Trudy MAI, 2017, no. 95. Available at: http://trudymai.ru/published.php?ID=83562 (accessed 26.05.2019) (In Russ.)

12. Akimov A. I. *Aerodinamika i letnyye kharakteristiki vertoletov* [Aerodynamics and Flight Characteristics of Helicopters]. Moscow, *Mashinostroyeniye*, 1988, 144 p. (In Russ.)

13. Volodko A. M., Verkhozin M. P., Gorshkov V. A. Vertolety: *Spravochnik po aerodinamike, dinamike poleta, konstruktsii, oborudovaniyu i tekhnicheskoy ekspluatatsii* [Helicopters: Handbook of Aerodynamics, Flight Dynamics, Design, Equipment and Technical Operation], ed. by A. M. Volodko. Moscow, *Voyenizdat,* 1992, 557 p. (In Russ.)

14. Mil' M. L., Nekrasov A. V., Braverman A. S., Grodko L. N., Leikand M. A. *Vertolety, raschet i proyektirovaniye. Tom 2. Kolebaniya i dinamicheskaya prochnost'* [Helicopters, Calculation and Design. Vol. 2. Oscillations and Dynamic Strength]. Moscow, *Mashinostroyeniye*, 1967, 424 p. (In Russ.)

15. Bullard B. D., Dowdy P. C. Pulse Doppler signature of a rotary-wing aircraft. IEEE Aerospace and Electronic Systems Magazine, 1991, vol. 6, iss. 5, pp. 28–30.

16. Fliss G. G. Tomographic Radar Imaging of Rotating Structures. Proc. SPIE 1630, Synthetic Aperture Radar, 1992, pp. 199–207.

17. Rotander C. E., Von Sydow H. Classification of Helicopters by the L/N-quotient. Proc. of the Radar 97 (Conf. Publ. 449), 1997, pp. 629–633.

18. Tikkinen J. M., Helander E. E., Visa A. Joint Utilization of Incoherently and Coherently Integrated Radar Signal in Helicopter Categorization. IEEE International Radar Conf., Arlington, VA, 9–12 May 2005, Piscataway, IEEE, 2005, pp. 540–545.

Sergey R. Heister – Dr. of Sci. (Engineering) (2004), Professor (2006). Head of experimental developments of Closed joint-stock company "Group of Manufacturing Technologies and Aeronautical Engineering AEROMASH". The author of more than 150 scientific publications. Area of expertise: construction of radio engineering systems for various purposes; radar recognition; adaptive signal processing; radioelectronic protective measures.
E-mail: hsr_1960@yahoo.com

Thai T. Nguyen – Master of engineering and technology (2016). Postgraduate student at the Department of Information radiotechnologies department of Belarusian State University of Informatics and Radioelectronics. The author of 14 scientific publications. Area of expertise: radar recognition; digital signal processing.
E-mail: thairti@gmail.com

СПИСОК ЛИТЕРАТУРЫ

1. Экспериментальное обоснование модели отраженного от вертолета радиолокационного сигнала / О. В. Васильев, П. В. Кутахов, В. Г. Щекотилов, И. А. Юрчик // Радиотехника. 2001. № 11. С. 12–16.

2. Радиолокационные характеристики летательных аппаратов / М. Е. Варганов, Ю. С. Зиновьев, Л. Ю. Астанин, А. А. Костылев, А. Я. Пасмуров, В. А. Сарычев, С. К. Слезкинский, Б. Д. Дмитриев.; под ред. Л. Т. Тучкова. М.: Радио и связь, 1985. 235 с.

3. Бартон Д. Радиолокационные системы; пер. с англ. П. Горохова, О. Казакова, А. Тупицына. М.: Воениздат, 1967. 480 с.

4. Радиоэлектронные системы. Основы построения и теория / Я. Д. Ширман, Ю. И. Лосев, Н. Н. Минервин, С. В. Москвитин, С. А. Горшков, Д. И. Леховицкий, Л. С. Левченко / под ред. проф. Я. Д. Ширмана / ЗАО "МАКВИС".М., 1998. 828 с.

5. Бакулев П. А. Радиолокация движущихся целей. М.: Сов. радио, 1964. 336 с.

6. Справочник по радиолокации: в 4 т.; под ред. М. Сколника. Т. 1. Основы радиолокации / пер. с англ.; под общ. ред. К. Н. Трофимова. М.: Сов. радио, 1976. 455 с.

7. Джонсон У. Теория вертолета: в 2 кн.; пер. с англ. Кн. 2. М.: Мир, 1983. 1024 с.

8. Юрьев Б. Н. Избранные труды: в 2 т. Т. 1. Воздушные винты. Вертолеты. М.: Изд-во АН СССР, 1961. 553 с.

9. Зозуля В. Б., Лалетин К. Н., Гученко Н. И. Практическая аэродинамика вертолета Ми-2. М.: Воздушный транспорт, 1984. 176 с.

10. Романчук В. Н., Красильников В. В. Вертолет Ми-2. М.: Транспорт, 1972. 260 с.

11. Борисов Е. А., Леонтьев В. А., Новак В. Н. Анализ особенностей работы несущего винта с отрицательным выносом горизонтальных шарниров // Тр. МАИ. 2017. № 95. URL: http://trudymai.ru/published.php?ID=84476 (дата обращения 26.05.2019)

12. Акимов А. И. Аэродинамика и летные характеристики вертолетов. М.: Машиностроение, 1988. 144 с.

13. Вертолеты: справ. по аэродинамике, динамике полета, конструкции, оборудованию и технической эксплуатации / А. М. Володко, М. П. Верхозин, В. А. Горшков; под ред. А. М. Володко. М.: Воениздат, 1992. 557 с.

14. Вертолеты, расчет и проектирование: в 3 т. Т. 2. Колебания и динамическая прочность / М. Л. Миль, А. В. Некрасов, А. С. Браверман, Л. Н. Гродко, М. А. Лейканд; под ред. М. Л. Миля. М.: Машиностроение, 1967. 424 с.

15. Bullard B. D., Dowdy P. C. Pulse Doppler signature of a rotary-wing aircraft // IEEE Aerospace and Electronic Systems Magazine. 1991. Vol. 6, iss. 5. P. 28–30.

16. Fliss G. G. Tomographic radar imaging of rotating structures // Proc. SPIE Vol. 1630, Synthetic Aperture Radar. 1992. P. 199–207. doi: 10.1117/12.59018

17. Rotander C. E., Von Sydow H. Classification of helicopters by the L/N-quotient // Proc. of the Radar 97 (Conf. Publ. 449), 14–16 Oct 1997, Edinburgh, UK. Piscataway: IEEE, 1997. P. 629–633.

18. Tikkinen J. M., Helander E. E., Visa A. J. E. Joint utilization of incoherently and coherently integrated radar signal in helicopter categorization // IEEE Intern. Radar Conf., 9–12 May 2005, Arlington, VA, USA. Piscataway: IEEE, 2005. P. 540–545. doi: 10.1109/RADAR.2005.1435885

Гейстер Сергей Романович – доктор технических наук (2004), профессор (2006). Руководитель опытных и экспериментальных разработок ЗАО "Группа производственных технологий и авиационного машиностроения Аэромаш". Автор более 150 научных работ. Сфера научных интересов – построение радиотехнических систем различного назначения; радиолокационное распознавание; адаптивная обработка сигналов; радиоэлектронная защита.
E-mail: hsr_1960@yahoo.com

Нгуен Тьен Тхай – магистр техники и технологии (2016), аспирант кафедры информационных радиотехнологий Белорусского государственного университета информатики и радиоэлектроники. Автор 14 научных работ. Сфера научных интересов – радиолокационное распознавание; цифровая обработка сигналов.
E-mail: thairti@gmail.com